Abrupt Structural Transformation in Hydrotalcite-like Compounds $Mg_{1-x}Al_x(OH)_2(NO_3)_x{\cdot}nH_2O$ as a Continuous Function of Nitrate Anions

Z. P. Xu and H. C. Zeng*

Department of Chemical and Environmental Engineering, Faculty of Engineering, National University of Singapore, 10 Kent Ridge Crescent, Singapore 119260

Received: August 10, 2000; In Final Form: December 8, 2000

We report here a systematic XRD/FTIR/CHN/ICP investigation for structural transformation of hydrotalcite-like compounds $Mg_{1-x}Al_x(OH)_2(NO_3)_x{\cdot}nH_2O$ as a continuous function of nitrate anions ($x = 0.18-0.34$). With seven finely divided steps in x value, a clear relationship between basal spacing and nitrate anion content (and thus trivalent cation content) has been found. In particular, we have been able to "arrest" an intermediate hydrotalcite-like phase that situates at the midpoint of an abrupt structural transformation. Unlike that of normal hydrotalcites, the relationship revealed in our nitrated $Mg_{1-x}Al_x(OH)_2(NO_3)_x{\cdot}nH_2O$ samples is much more complicated. While the lattice parameter a decreases with increase of nitrate content, the parameter c decreases slightly over $x = 0.18-0.22$, rises abruptly with a further increase of nitrate anions at $x = 0.26$, and then reaches maximums at $x = 0.31-0.34$. The compound at $x = 0.26$ also shows a sharp decrease in mean crystallite dimension. The abrupt structural change is attributed to a drastic change in nitrate anion arrangement. On the basis of our FTIR observations and Coulombic energy estimation, a "stick-lying" model for nitrate arrangement has been proposed, which is apparently superior to a "tilt-lying" model reported previously. The saturated charge density of the brucite-like layers for the "stick-lying" nitrate anions is about 4 e/nm^2. The sharp decrease in crystallite dimension can be ascribed to the change of nitrate configuration from "flat-lying" to "stick-lying" due to increasing lateral repulsion among the anions and thus discontinuation in the planar growth.

Introduction

Layered double hydroxides (LDHs) are important clay materials owing to their intercalation ability of anionic species and other physicochemical properties for applications as anion adsorbents, medicine stabilizers, ion-exchangers, ionic conductors, catalysts and catalyst supports,[1−6] and even nanocarbon fabrication.[5d] Among these interesting layered materials, hydrotalcite-like compounds (HTlcs), in particular, have attracted considerable attention in the past two decades.

In the hydrotalcite-like compound, a divalent metal cation is located in the center of oxygen octahedron constructed by six hydroxyl groups. The resultant octahedrons are connected one another by edge-sharing to form two-dimensionally infinite sheets (or layers), which is similar to the basic structure of brucite $Mg(OH)_2$.[1] The brucite-like layers can stack upon one another to form a three-dimensional solid owing to various chemical interactions between the layers. Nonetheless, if some of the divalent cations in the octahedrons are substituted by trivalent ones, organic or inorganic anions including oxometalates will be intercalated into the space between brucite-like layers (or gallery space) to compensate extra cationic charges possessed by the trivalent cations in the brucite-like layers. Therefore, this anion intercalation process during the compound preparation leads to the formation of a hydrotalcite-like structure, which is named after the natural hydrotalcite compound, $Mg_6Al_2(OH)_{16}CO_3{\cdot}4H_2O$.[1]

The exact structure of HTlcs was determined only in the late 1960s,[7] although the chemical formula for the hydrotalcite had been known as early as in 1915.[8] One of the most important structural properties of HTlcs is the distance between two neighboring brucite-like layers (i.e., the basal spacing), which is related to their ability of anion intercalation. Because of variation in natures of anions in gallery space and cations in brucite-like layers, such as in size and charge, the basal spacing of the compounds is expected to change accordingly. Nonetheless, due to the complexity in synthetic methods, this common expectation has not been always realized.

For the hydrotalcite compounds ($MgAl-CO_3-HT$) synthesized individually, the basal spacing does not show a clear relationship with trivalent content (x), as different research groups have their own preferred or modified synthetic conditions. For example, a variation of 0.2 Å in d_{003} is observed even with the similar x values.[9−12] When the hydrotalcite compounds are studied as a function of intercalated anion, the relationship between the basal spacing and the x value becomes clearer, although different methods produce different sets of basal spacing.[13] It is found that the basal spacing decreases when x value increases.[13−17] The general trend observed is attributed to the increase in electrostatic interaction between the brucite layers and the anions intercalated that reduces the basal spacing. However, controversial results in basal spacing at low x value region are still noted.[15−17] For example, a local maximum of 7.98 Å at $x = 0.170$ has been observed,[17] while others show a straight linear relationship over the same x range.[15,16] Similar to the standard hydrotalcites, transition-metal substituted derivatives $MAl-CO_3-HT$ (M = Ni, Zn, Co) show a similar relationship between the basal spacing and trivalent content.[18−25]

In comparison to the above carbonated HTlcs that have been investigated in great detail, the study of nitrated HTlcs has been

* To whom correspondence should be addressed.Tel: +65 874 2896. Telefax: +65 779 1936. E-mail: chezhc@nus.edu.sg.

10.1021/jp0029257 CCC: $20.00
Published on Web 02/10/2001

TABLE 1: Elemental Analysis Results and Chemical Formulas for the Synthesized Compounds

sample	x_{ini}[a]	x[b]	A/M[c]	Mg %[d]	Al %[d]	N %[d]	C %[d]	phase	chem formula
HT1	0.13	0.18	0.21	21.7	5.4	2.80	0.16	HT[e]	$Mg_{0.82}Al_{0.18}(OH)_{1.97}(NO_3)_{0.18}(CO_3)_{0.015}\cdot 1.1H_2O$[e]
HT2	0.17	0.20	0.22	22.5	6.1	3.10	0.16	HT	$Mg_{0.80}Al_{0.20}(OH)_{1.98}(NO_3)_{0.19}(CO_3)_{0.015}\cdot 0.9H_2O$
HT3	0.20	0.22	0.23	22.0	6.9	3.40	0.16	HT	$Mg_{0.78}Al_{0.22}(OH)_{1.99}(NO_3)_{0.20}(CO_3)_{0.015}\cdot 0.8H_2O$
HT4	0.25	0.26	0.25	22.0	8.8	4.16	0.08	HT	$Mg_{0.74}Al_{0.26}(OH)_{2.01}(NO_3)_{0.24}(CO_3)_{0.005}\cdot 0.4H_2O$
HT5	0.30	0.31	0.31	20.0	10.2	5.04	0.08	HT	$Mg_{0.69}Al_{0.31}(OH)_{2.00}(NO_3)_{0.30}(CO_3)_{0.005}\cdot 0.3H_2O$
HT6	0.33	0.34	0.33	29.0	10.7	5.12	0.16	HT	$Mg_{0.66}Al_{0.34}(OH)_{2.00}(NO_3)_{0.31}(CO_3)_{0.01}\cdot 0.3H_2O$
HT7	0.40	0.40	0.30	18.0	13.2	4.56	0.16	HT[f]	$Mg_{0.60}Al_{0.30}(OH)_{1.80}(NO_3)_{0.28}(CO_3)_{0.01}\cdot 0.2H_2O$[f]

[a] x_{ini} is the molar ratio of trivalent cations to total cations in initial solutions; $x_{ini} = [Al^{3+}]/([Mg^{2+}] + [Al^{3+}])$. [b] x is the molar ratio of trivalent cations to total cations in as-prepared solid samples; $x = Al^{3+}/(Mg^{2+} + Al^{3+})$. [c] A/M is the molar ratio of $(NO_3^- + 2CO_3^{2-})/(Mg^{2+} + Al^{3+})$ in solid samples. [d] Elemental analysis by ICP and CHN in weight percentage. [e] This sample may contains a trace amount of $Mg(OH)_2$ (see text). [f] This sample contains 10 mol % of total cations in $Al(OH)_3$ phase (see text). The chemical formula can also be written as $Mg_{0.67}Al_{0.33}(OH)_{2.00}(NO_3)_{0.31}(CO_3)_{0.01}\cdot 0.2H_2O$, where the total molar number of cations is normalized to 1.00, as for HT1−HT6.

less systematic although the nitrate anion has a geometrical configuration similar to that of the carbonate and is the second most common anion in the HTlcs. In most cases, only one or two compounds have been prepared and the agreement among these data is not obvious. Although in some cases the range of x value is larger ($x = 0.20-0.33$),[26] the distribution of data does not give a definite trend. Similar to these $MgAl-NO_3-$HTlcs, the transition-metal-substituted nitrated HTlcs represent another case of the uncertainty and contraversy.[18,23,27,28]

Apart from the errors in experimental measurement, the major difficulties in finding the relationship between basal spacing and trivalent content for the HTlcs are the following: (i) formation of secondary phases which results in an insufficient x coverage to observe an entire structural transformation; (ii) determination of chemical composition of HTlcs, since anions with high affinity in interlayer space such as carbonates cause a significant reduction in basal spacing even if the ratio of $M^{III}/(M^{II}+M^{III})$ has been known; (iii) low crystallinity which lowers accuracy of spacing data. To gain a better understanding on the intercalation process of nitrate anions, in this paper, we report a systematic XRD/FTIR/CHN/ICP investigation for the structural transformation of $MgAl-NO_3-$HTlcs.

Experimental Section

Sample Preparation. A coprecipitation method was used to prepare MgAl-hydrotalcite-like compounds intercalated with nitrate anions. Briefly, 20.0 mL of salt solution containing $Mg(NO_3)_2\cdot 6H_2O$ (Merck, 99%) and $Al(NO_3)_3\cdot 9H_2O$ (Merck, 98.5%) was added dropwise within 10 min into a rigorously stirred ammoniacal solution (100.0 mL, 0.5 M). The total cation concentration was kept at 1.0 M for all 7 samples while the molar ratio of cations $[Al^{3+}]/([Mg^{2+}] + [Al^{3+}])$ was varied as indicated in Table 1. The sample names are designated sequentially according to the content of trivalent cation Al^{3+}. After being aged at 65 °C for 18 h, the mixture was then filtered and washed thoroughly with deionized water, followed by a drying overnight in vacuo at room temperature.

Characterization Techniques. Crystallographic information on the samples was investigated by powder X-ray diffraction (XRD). Diffraction patterns of intensity-versus-two-theta (2θ) were recorded with a Shimadzu XRD-6000 X-ray diffractometer using Cu Kα radiation ($\lambda = 1.5418$ Å) at a scanning rate of 1° min^{-1}. The interplanar spacing of the resultant HTlcs was determined from the diffraction peak positions/patterns with structural analysis software. Chemical bonding information on metal−oxygen, hydroxyl, and intercalated anion (such as NO_3^-) was obtained with Fourier transform infrared spectroscopy (FTIR, Bio-Rad, model FTS 3500) using the potassium bromide (KBr) pellet technique. Each FTIR spectrum was collected after 40 scans with a resolution of 4 cm^{-1}. Carbon and nitrogen contents of the as-prepared hydrotalcite-like compounds were measured in a Perkin-Elmer 2400 CHN analyzer, while the magnesium and aluminum contents were determined by inductively coupled plasma (ICP) emission spectroscopy (Perkin-Elmer ICP OPTIMA-3000).

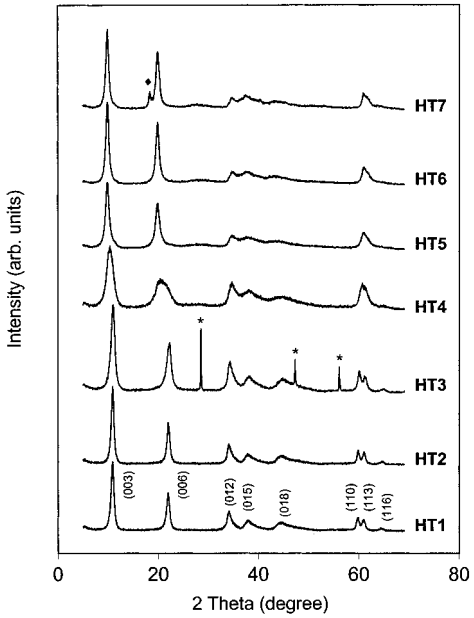

Figure 1. XRD patterns of as-prepared samples HT1−HT7. The ◆ sign in the HT7 pattern indicates the presence of $Al(OH)_3$, and the * signs are the reflections from polycrystalline silicon used as an internal standard.

Results and Discussion

Formation of HTlcs and Compositional Analysis. The X-ray diffraction patterns of the as-prepared samples are shown in Figure 1, which confirms the formation of hydrotalcite-like structure in all compounds. The diffraction peaks are indexed according to the 3R symmetry.[1,2,30] The general trend observed is that the (003) and (006) peaks shift to smaller 2θ angles when x value is increased in the sequence from HT1 to HT7. The HT4 sample, in particular, is located in the midpoint of this transition, which divides the XRD patterns into two different groups. For example, after HT4, the (003) and (006) peaks of samples HT5 to HT7 become narrow again although the other peaks are still broad, and especially, the (110) and (113) peaks become seriously overlapped. It is also observed that sample HT7, which contains 40 mol % of Al^{3+} in total metal cations, exhibits an extra peak at 18.4° due to the presence of $Al(OH)_3$ (in Gibbsite phase).[31]

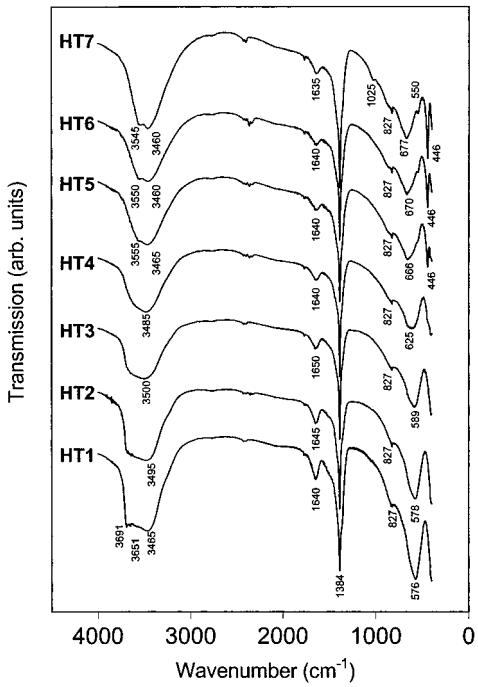

Figure 2. FTIR spectra of as-prepared hydrotalcite-like samples HT1−HT7.

Table 1 summarizes the results of elemental analysis. It is noted that the trivalent cation molar fraction (x) in the precipitates is in good agreement with that in the initial solution (x_{ini}) except for sample HT1. Since an extra amount of Mg^{2+} was used in this sample, where x_{ini} is smaller than required values (0.2−0.4) for the formation of pure HTlcs, brucite $Mg(OH)_2$ may be formed. However, due to the relatively high solubility of $Mg(OH)_2$ ($K_{sp} = 7.1 \times 10^{-12}$),[32] a considerable amount of Mg^{2+} cations (ca. 20%) that should be precipitated actually remains in the weak base solution (final pH = 8.5−9.0). In fact, this expectation is true because no XRD pattern of the brucite phase can be found in HT1 and only a trace amount of high-basicity O−H has been detected in our FTIR measurement, which will be presented shortly.

The negative charges (which is the same as the A/M ratio in Table 1) in the gallery space are noted to balance very well with the positive ones in the brucite-like layers (x), as expected to have an electric neutrality for the formation of HTlcs. The only exception observed in the sample of HT7, where x (0.40) is greater than A/M (0.30, Table 1), is caused by the formation of a secondary phase, $Al(OH)_3$,[31] as revealed by the XRD patterns in Figure 1. The above-prepared samples have been further chemically formulated in Table 1, on the basis of the elemental analyses (CHN and ICP) and the total charge balance.

The changes of FTIR spectra of the as-prepared HTlcs in the sequence of their trivalent Al^{3+} content are shown in Figure 2. The most prominent feature for this spectral evolution is that there is an intensive sharp peak at 1384 cm^{-1} (due to ν_3 vibrational mode of NO_3^- with D_{3h} symmetry) that shows no peak shift. Similarly, a weak peak at 827 cm^{-1} caused by the ν_2 mode of the same anion also shows no shift in all spectra.[5,6,33−38] The constant wavenumbers of these two modes have indicated that nitrate anions in the gallery space are relatively unperturbed, keeping their D_{3h} symmetry. An important exception comes from the HT7 spectrum, where IR-inactive ν_1 mode under the D_{3h} symmetry becomes active, as shown by the weak peak at 1025 cm^{-1}. This is indicative of a symmetry lowering to C_{2v} (ν_2 mode)[33] when the content of nitrate anions reaches its upper limit in the gallery space, which will be further addressed in later subsections.

Much more information can also be attained from the various vibrations of hydroxyl groups. A broad band of the ν_{OH} stretching is obviously noted at around 3500 cm^{-1} for all the samples.[5,6,35,37,39] It has been known that, for the pure $Mg(OH)_2$, a single band at 3698 cm^{-1} is recorded owing to high basicity of its O−H groups.[40] The tiny tips at high wavenumbers of 3691 and 3651 cm^{-1} in the spectrum of HT1 can be attributed to possible existence of trace brucite compound $Mg(OH)_2$ although the XRD patterns (Figure 1) do not suggest this phase. Surprisingly, for samples HT5−HT7, the broad band of O−H becomes narrower and separates into two components, as shown in a new band appearing at the 3545−3555 cm^{-1} region. It is important to mention that another broad band at low-wavenumber region, owing to the δ-mode of the O−H groups, drastically changes its position from 576 to 677 cm^{-1} for HT1−HT7.[34,41] The gradual decrease in intensity of the peak at 1635−1650 cm^{-1} (due to the δ_{HOH} mode of water molecules)[39] is in good agreement with the decrease of water content from samples HT1−HT7 (chemical formulas, Table 1).

Some lattice vibrations of metal−oxygen bonds M−O are also observed at 550 and 446 cm^{-1}.[42,43] It is possible that some of them are overlapped with the broad band (δ-mode of the O−H) or take place at even lower wavenumber region beyond the measured range.

Structural Transformations upon Anion Intercalation. To quantitatively evaluate the change of lattice parameters (such as c and a) of the prepared HTlcs, polycrystalline silicon powder has been used as an internal standard for diffraction angle calibration, as indicated in the XRD patterns of sample HT3 in Figure 1. As mentioned earlier, the peaks of (110) and (113) in the XRD patterns are overlapped, especially in the samples of HT4−HT7. To obtain a values that are calculated from the (110) peaks, the deconvolution of the two overlapped peaks is carried out by a computer program without setting any peak-width constraints, as shown by the three examples in Figure 3.

On the basis of the 2θ angles of (003) and (110) peaks, the lattice parameters c ($=3d_{003}$) and a ($=2d_{110}$) are calculated and listed in Table 2. The changing pictures with the trivalent content (x) are further plotted in Figure 4. It is clear that the parameters c and a greatly change with the increase of trivalent Al^{3+} in the brucite-like layers, but seemingly each follows an opposite trend. The parameter a, i.e., the shortest distance between two metal cations in the same brucite-like layer, decreases with the increase of trivalent cation content, showing the same trend as reported for $MgAl-CO_3$–HTlcs.[1,15,16,44] This change is attributed to an increase of attractive interaction within the brucite-like layer when more Al^{3+} cations are incorporated.[1,15,16] On the other hand, the parameter c decreases slightly in the first three samples ($x = 0.18-0.22$), i.e., from HT1 to HT3. This decrease has also been observed for $MgAl-CO_3$−HTlcs in a very wide range ($x = 0.1-0.65$ in the initial solution).[1,15,16,22] Nevertheless, this parameter rises abruptly with the further increase of the trivalent cations and quickly reaches a maximum value, 26.86 Å, in sample HT7. This observation is totally different from the findings for $MgAl-CO_3$−HTlcs and will be addressed in detail shortly.

Charge Density Considerations. In contrast to the changes of lattice parameters, the changes of the mean crystallite dimension (thickness) in the [003] and [110] directions (D_{003} and D_{110} in Table 2) follow the same trend, i.e., being larger at low and high x values but smaller in the middle x range, as shown in two V-shaped curves in Figure 5. The variation in

TABLE 2: Changes of Lattice Parameters and Crystallite Size with Trivalent Content *x*

sample	x[a]	*c* (Å)	*a* (Å)	d_{003} (Å)	size in *c*-axis (nm)[b]	size in *a*-axis (nm)[c]
HT1	0.18	24.48	3.092	8.16	11.4	13.5
HT2	0.20	24.40	3.088	8.13	12.5	17.3
HT3	0.22	24.23	3.078	8.08	8.5	12.7
HT4	0.26	25.48	3.056	8.49	4.0	9.1
HT5	0.31	26.84	3.046	8.95	9.0	10.7
HT6	0.34	26.83	3.040	8.94	10.9	12.0
HT7	0.33	26.86	3.041	8.95	10.7	13.2

[a] Molar ratio of trivalent cations to total cations in the hydrotalcite-like compounds of Table 1, $x = Al^{3+}/(Mg^{2+} + Al^{3+})$. [b] Mean crystallite size calculated from full width of half-maximums (fwhms) of (003) peaks. [c] Mean crystallite size calculated from fwhms of (110) peaks.

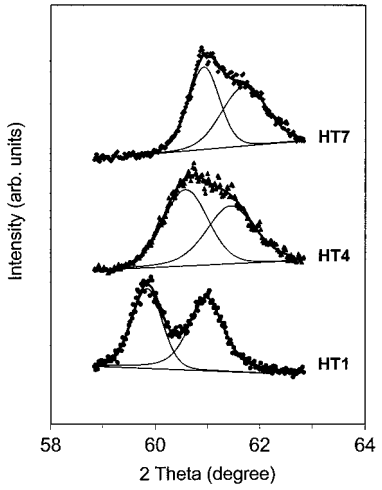

Figure 3. Deconvolution of (110) and (113) peaks for three representative samples HT1, HT4, and HT7.

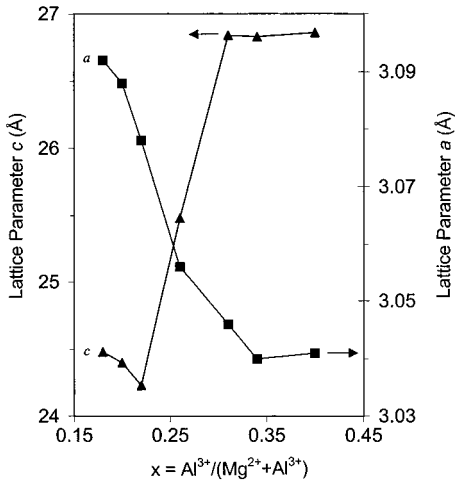

Figure 4. Abrupt changes of lattice parameters (*c* and *a*) versus molar ratio of trivalent cations to total cations, noting that HT4 sample is located in the juncture ($x = 0.26$) of the two opposite transitions.

crystallite dimension is significant, up to 2−3 times within each curve. The turning point corresponding to the smallest crystallite size is around $x = 0.26$ (sample HT4), where the lattice parameters have also shown a juncture at this *x* value (Figure 4). As a rough estimation, the mean volume of crystallite in each sample can be calculated on the basis of the disklike morphology (hexagonal area · height)[9b,45] for the HTlcs:

$$V = \pi r^2 h = \pi(^1/_2 D_{110})^2 D_{003} \quad (1)$$

Here a round area πr^2 has been used as an approximation for the hexagonal area. A more accurate estimation can be obtained using the volume ratio of eq 1, which shows that the largest mean crystallite in HT2 is over 10 times of that in HT4.

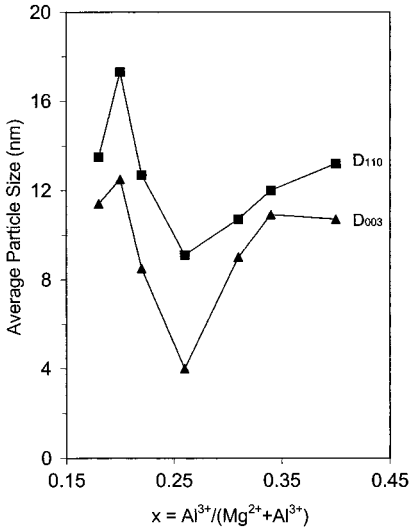

Figure 5. Profiles of average crystallite size versus molar ratio of trivalent cations to total cations. D_{003} and D_{110} are calculated from fwhms of (003) and (110) peaks, respectively.

A calculation of the charge density that influences nitrate anion orientation may provide some clues to explain the observed V-shaped changes of the mean crystallite size and thus the crystallite growth. As the cation ratio and the lattice parameters are determined in the previous section, the area that contains one positive charge ($S_{unit-charge}$) or the positive charge density (d_c) in the brucite-like layer can thus be calculated:

$$S_{unit-charge} = a^2 \sin 60°/xe \quad (2)$$

$$d_c = 1/S_{unit-charge} = xe/a^2 \sin 60° \quad (3)$$

Here *a* is the lattice parameter in brucite-like layer, *x* the molar ratio of trivalent to total cations, and *e* the charge of an electron. Since the parameter *a* is relatively constant (Table 2), the charge density d_c changes smoothly upon the trivalent cation content (*x*), which shows a gradual increase from 2.2 to 4.2 *e*/nm^2 (HT1 to HT6, Table 3).

To evaluate the maximum dimension in the gallery available for the anions in our present samples, the anion (NO_3^- and CO_3^{2-}) are assumed to be lying flatly (parallel to the brucite-like layer) and occupying an allocated area which is normalized to a square with the side length of L_{NO_3} or L_{CO_3}, respectively. These calculated data are also listed in Table 3 for comparison. As can be seen, L_{CO_3} is about 40% longer than its corresponding L_{NO_3} due to the fact that the number of the divalent anions is only half of that of the monovalent anions.

In comparison with the above data, the dimension parameters of NO_3^- and CO_3^{2-} are also estimated and listed in Table 3. The area occupied by an anion is calculated from a contact rectangle model, where the contact radius (van der Waals radius)

TABLE 3: Area/Unit Charge, Charge Density of Brucite-like Layer, and Dimensions Available for the Intercalated NO_3^- and CO_3^{2-} Anions

sample	x[a]	$S_{unit-charge}$ (Å^2/e)[b]	d_c (e/nm^2)	L_{NO_3} (Å)	L_{CO_3} (Å)
HT1	0.18	46.0	+2.17[c]	6.78[d]	9.59[d]
HT2	0.20	41.3	+2.42	6.43	9.09
HT3	0.22	37.2	+2.69	6.10	8.63
HT4	0.26	30.8	+3.25	5.55	7.85
HT5	0.31	25.7	+3.90	5.07	7.16
HT6	0.34	23.6	+4.24	4.85	6.87
HT7	0.33	24.3	+4.12	4.93	6.97
NO_3^-	[area = 4.95 × 4.66 = 23.1 (Å^2)]		−4.34[e]	4.80[f]	
CO_3^{2-}	[area = 5.07 × 4.76 = 24.1 (Å^2)]		−8.29[e]		4.91[f]

[a] Molar ratio of trivalent cations to total cations in the hydrotalcite-like compounds of Table 1, $x = Al^{3+}/(Mg^{2+} + Al^{3+})$. [b] Surface area/unit of charge in the brucite-like layer (eq 2). [c] Charge density of the brucite-like layer (eq 3). [d] Normalized side length of a square area available in the gallery space for an anion to occupy: $L_{NO_3} = \sqrt{S_{unit-charge}}$ and $L_{CO_3} = \sqrt{2S_{unit-charge}}$. [e] Charge density of an anion (charge(s)/anion area). [f] Normalized side length of a square whose area is equal to the area of an anion.

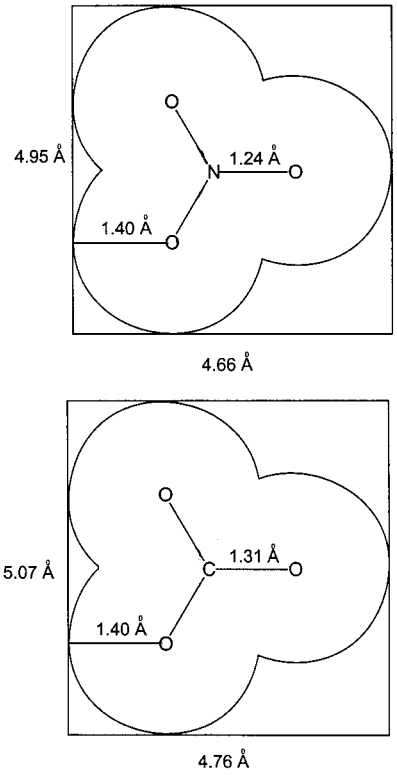

Figure 6. Planar geometries of two anions: NO_3^- and CO_3^{2-} (C_3 axis of the anions perpendicular to the paper).[46,47]

of oxygen is 1.40 Å, as shown in Figure 6.[46,47] Furthermore, the actual rectangles are also normalized to a square with the mean side length (also indicated by L_{CO_3} and L_{NO_3}, respectively), noting that this side length may represent a minimum distance between two anions with flat-lying configuration in the gallery space. Therefore, the charge density of anions (also indicated by d_c but with a negative value) should indicate a maximum value for this anion configuration. However, it is noted that d_c and L_{NO_3} of samples HT6 and HT7 have almost reached this limit (Table 3), indicating that the true structures in these samples have not been described adequately when we assume the simple flat-lying configuration for the studied anions.

Orientations of Nitrate Anions in the Gallery. Several features on the MgAl−NO_3−HTlcs can now be outlined: (i) NO_3^- anions in the gallery space are in a relatively unperturbed state with D_{3h} symmetry except for sample HT7 in which some low-symmetry vibrations of NO_3^- anions can be observed. (ii) The hydroxyl groups in the brucite-like layers have two different chemical environments, especially for the samples with higher

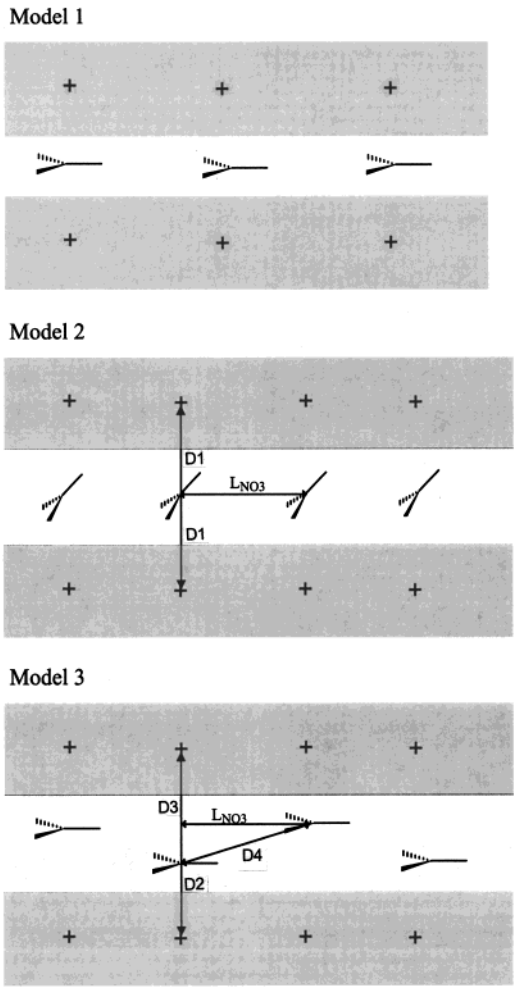

Figure 7. Three structural models regarding the arrangement of nitrate anions in samples HT1−HT7: (1) flat-lying model; (2) tilt-lying model; (3) stick-lying model.

x values. (iii) When x reaches around 0.26, the basal spacing abruptly increases, accompanied by a sharp decrease in crystallinity. All these features indicate a significant structural change in these samples upon a smooth increase in anion content. The abrupt change in structure, in turn, should be attributed to a sudden change of the intercalated nitrate anions in their structural arrangement in the gallery space.

For the nitrate anions, there are three possible arrangements in the gallery as shown in Figure 7. The first one is a flat-lying model, in which the NO_3^- anions are evenly located around the middle of the gallery and their molecular planes are parallel

TABLE 4: Comparison in Electrostatic Interaction between the Flat-Lying and Stick-Lying Models Using the Compositional/Structural Data for the HT2 and HT6 Samples, Respectively

sample	type of interaction	tilt-lying model	stick-lying model	energy ratio
HT2	attraction[a]	$D_1 = 4.065$ Å	$D_2 = 3.80$ Å $D_3 = 4.33$ Å	EA_S/EA_T[c] = 1.004
	repulsion[b]	$L_{NO_3} = 6.43$ Å	$D_4 = 6.45$ Å	ER_S/ER_T[d] = 0.997
HT6	attraction[a]	$D_1 = 4.47$ Å	$D_2 = 3.80$ Å $D_3 = 5.14$ Å	EA_S/EA_T[c] = 1.023
	repulsion[b]	$L_{NO_3} = 4.85$ Å	$D_4 = 5.03$ Å	ER_S/ER_T[d] = 0.964

[a] The attraction interaction between an anion and two cations (up and down) in the brucite-like layers. [b] The repulsion interaction between two anions in the same gallery space. [c] The ratio of attraction energies of stick-lying model (S) to tilt-lying model (T). [d] The ratio of repulsion energies of stick-lying model (S) to tilt-lying model (T).

to the brucite-like layers (model 1). This structure is identical to that of the hydrotalcite compounds MgAl−CO_3−HTlcs. When the charge density is low, such as in the samples HT1 and HT2 (where $x = 0.18$ and 0.20), L_{NO_3} value (6.78−6.43 Å) is very close to that of carbonate-containing HTlcs with high x values (e.g., flat-lying CO_3^{2-} in MgAl−CO_3−HTlcs, $x = 0.33-0.37$;[9a,13,14] refer to $L_{CO_3} = 6.87$ Å for $x = 0.34$ in Table 3). In comparison, it seems that there is sufficient space for the nitrate anions to adopt the flat-lying configuration at low x values since the number of anions in the gallery space is low.

However, our calculated side length and charge density in Table 3 do not suggest this model for the nitrate-containing HTlcs with high x values. This is because the gallery space is insufficient for all monovalent anions to be accommodated in this way. The strong repulsion among nitrate anions forces the anions to adjust in the orientation. Therefore a tilt-lying model has been considered, as shown in Figure 7 (model 2). The tilt-lying model had been actually proposed in the studies of NiAl−NO_3−HT,[18] NiAl−CO_3−HT,[19] and MgAl−NO_3−HT.[29d] In this model, NO_3^- anions are tilted with a slant angle in the gallery space but could not stand vertically because of limited height of the gallery. A simple summation of short side length of NO_3^- (4.66 Å, Figure 6)[46,47] and the thickness of brucite-like layer (4.80 Å) will give a basal spacing of 9.46 Å, or 0.51 Å more than the observed value 8.95 Å for HT5−HT7 (Table 2). According to this model, the slant angle and thus the basal spacing will be gradually increased when the charge density increases, although there is a limit of this angle at $\leq 90°$ (i.e., basal spacing of 9.46 Å when the slant angle = 90°). Nevertheless, such a smooth increase in basal spacing is not observed. Instead, there is only an abrupt jump in the basal spacing. It should be pointed out that the slant NO_3^- or CO_3^{2-} anions will not retain D_{3h} symmetry but change to C_{2v} symmetry,[19] which is clearly not the case in our FTIR investigation (no detection of the ν_1, ν_2, and ν_4 modes in C_{2v},[19,33−38] Figure 2). Furthermore, the crystallite size data also indicate there is a lack of smooth transformation in the compounds synthesized; even the anions are intercalated gradually as a continuous function. Apparently, all our experimental observations do not suggest the tilt-lying model for the nitrate-containing HTlcs at high x values. Therefore, this anion arrangement could be ruled out.

In Figure 7 (Model 3), we propose a new model for the anion arrangement. In this "stick-lying" model, nitrate anions alternatively stick to the top and bottom planes of the same gallery, which allows the anions to retain a D_{3h} symmetry. According to this model, surprisingly, the hydroxyl groups of the brucite-like layers can be divided into two classes: one directly contacts with nitrate anions and the other does not. With this configuration, the OH groups that do not directly interact with NO_3^- will show higher wavenumber, which is in excellent agreement with the experimental observation that there is a new component in OH bands in our FTIR spectra for the samples HT5−HT7. The "stick-lying" model is also advantageous in lowering the electrostatic energy. Using the compound of HT6 as a simple demonstration, the point charge interaction (from Coulomb's law) is adopted for an energy estimation of some nearest point charges, and resultant data are tabulated in Table 4. We find that the attractive energy (negative) is increased by 2.3% ("pulling") while the repulsive energy (positive) is released by 3.6% ("pushing") in the stick-lying model, compared to those in the tilt-lying configuration. Thus the total electrostatic interaction energy (negative) will be lower by more than 6% than that in the tilt-lying model. For sample HT2 ($x = 0.20$), on the other hand, the "pulling and pushing" effect can be ignored since its energy gain or loss is only around 0.4% (Table 4). This may further support that the flat-lying model is valid in the lower x cases (HT1−HT3). However, the above effect is starting in sample HT4, since its $x = 0.26$, $d_c = 3.25$ e/nm^2, and $L_{NO_3} = 5.55$ Å (Table 3) are close to the saturated values, i.e., the ratios d_c(HT4)/d_c(NO_3^-) = 0.75 and L_{NO_3}(HT4)/L_{NO_3}-(NO_3^-) = 1.16, noting that the both ratios are around the unity. If we treat the data reported for the compound NiAl−CO_3−HT [where $x = 0.44$, $d_c = 5.50$ e/nm^2, and $L_{CO_3} = 6.03$ Å, i.e., the ratios d_c(NiAl−CO_3−HT)/d_c(CO_3^{2-}) = 0.66 and L_{CO_3}-(NiAl−CO_3−HT)/L_{CO_3}(CO_3^{2-}) = 1.23; the relevant data d_c and L_{CO_3} here are calculated accordingly][19] as limits for a flat-lying anion-arrangement, it is then clear that HT4 has to adopt a different arranging manner because of higher charge density and less space (i.e., d_c ratios, 0.75 > 0.66, and length ratios, 1.16 < 1.23). It has been known that the mobility of interlayer nitrate in hydrotalcite-like phase is intermediate between that of carbonate and chloride.[29e,48,49] A recent NMR investigation indicates a rapid 3-fold rotation of nitrate anions in the gallery space at −100 to +80 °C and relative humidities from 0 to 100% (at room temperature).[29e] Our proposed stick-lying model seems to support this rotation mechanism, since it is able to provide a highly symmetrical environment for nitrate anions.

As the initial trivalent cation ratio increases further, such as in HT7, the charge density on the brucite-like layers will reach a saturation value, which is determined by the ability of the accommodation of nitrate anions in the gallery and the liability of $Al(OH)_3$ formation. On the basis of our experiments, the saturated charge density is about 4 e/nm^2 for the nitrate-containing HTlcs (Table 3).

As for the abnormal decrease of the crystallite size occurring at $x = 0.26$, it is our belief that this is the transition point for nitrate anions from the flat-lying to stick-lying configuration due to the increase in lateral repulsion in the gallery space, which leads to a retardation of the planar growth for the brucite-like layers. Accordingly, the growth in c-axis is also suppressed due to the small size of brucite-like layers and the dimension requirement for disklike crystallite morphology.

Conclusions

In summary, relationships of lattice parameters and nitrate (and similarly Al^{3+}) content of the hydrotalcite-like compounds $Mg_{1-x}Al_x(OH)_2(NO_3)_x \cdot nH_2O$ ($x = 0.18-0.34$) have been revealed in this work. Although charge density (positive) of the brucite-like layers changes linearly among these samples (positive charge: 2.2−4.2 e/nm^2), the basal spacing does not show a smooth increase when the negative nitrate anions are intercalated accordingly. Lattice parameter a decreases with the increase of nitrate content. The parameter c, on the other hand, decreases slightly over $x = 0.18-0.22$, rises abruptly with further increase of nitrate anions at $x = 0.26$, and rapidly reaches maximums at $x = 0.31-0.34$. Data of mean crystallite dimension also show a drastic change for the sample at $x = 0.26$. The abrupt structural change can be attributed to a drastic change in nitrate anion arrangement, although the nitrate anion still maintains its D_{3h} symmetry. On the basis of the FTIR observations (of O−H and NO_3^-) and Coulombic energy estimation, the "stick-lying" model serves as a better description for the observed structural changes. The saturated charge density in the brucite-like layers for the "stick-lying" nitrate anions is about 4 e/nm^2. The sharp decrease in crystallite size at $x = 0.26$ can be attributed to the change of nitrate anions from "flat-lying" to "stick-lying" arrangement due to increasing lateral repulsion among the nitrate ions, which leads to discontinuation in planar growth of the brucite-like layers for the compound situates at the juncture of structural transition.

Acknowledgment. The authors gratefully acknowledge research funding (Grants R-279-000-064-112 and A/C50384) cosupported by the Ministry of Education and the National Science and Technology Board, Singapore.

References and Notes

(1) Cavani, F.; Trifiro, F.; Vaccari, A. *Catal. Today* **1991**, *11*, 173.
(2) Rives, V.; Ulibarri, M. A. *Coord. Chem. Rev.* **1999**, *181*, 61.
(3) Reiche, W. T. *Solid State Ionics* **1986**, *22*, 133.
(4) (a) Armor, J. N.; Braymer, T. A.; Farris, T. S.; Li, Y.; Petrocelli, F. P.; Weist, E. L.; Kannan, S.; Swamy, C. S. *Appl. Catal., B* **1996**, *7*, 397. (b) Hermosin, M. C.; Pavlovic, J.; Ulibarri, M. A.; Cornejo, J. *Water Res.* **1996**, *30*, 171.
(5) (a) Qian, M.; Zeng, H. C. *J. Mater. Chem.* **1997**, *7*, 493. (b) Xu, Z. P.; Zeng, H. C. *Chem. Mater.* **1999**, *11*, 67. (c) Xu, Z. P.; Zeng, H. C. *J. Mater. Chem.* **1998**, *8*, 2499. (d) Xu, Z. P.; Zeng, H. C. *J. Phys. Chem. B* **2000**, *104*, 10206.
(6) Chisem, I. C.; Jones, W. *J. Mater. Chem.* **1994**, *4*, 1737.
(7) (a) Allmann, R. *Acta Crystallogr.* **1968**, *B24*, 972. (b) Taylor, H. F. W. *Miner. Magn.* **1969**, *37*, 338.
(8) Manasse, E. *Atti Soc. Toscana Sci. Nat., P. V.* **1915**, *24*, 92.
(9) (a) Costantino, U.; Marmottini, F.; Nocchetti, M.; Vivani, R. *Eur. J. Inorg. Chem.* **1998**, 1439. (b) Cai, H.; Hillier, A. C.; Franklin, K. R.; Nunn, C. C.; Ward, M. D. *Science* **1994**, *266*, 1551.
(10) Marino, O.; Mascolo, G. *Proceedings of 2nd European Symposium on Thermal Analysis*; 1981; p 391.
(11) Ookubo, A.; Ooi, K.; Hayashi, H. *Langmuir* **1993**, *9*, 1418.
(12) Tanaka, M.; Park, I. Y.; Kuroda, K.; Kato, C. *Bull. Chem. Soc. Jpn.* **1989**, *62*, 3442.
(13) Yun, S. K.; Pinnavaia, T. J. *Chem. Mater.* **1995**, *7*, 348.
(14) (a) Bellotto, M.; Rebours, B.; Clause, O.; Lynch, J.; Bazin, D.; Elkaim, E. *J. Phys. Chem.* **1996**, *100*, 8527. (b) Bellotto, M.; Rebours, B.; Clause, O.; Lynch, J.; Bazin, D.; Elkaim, E. *J. Phys. Chem.* **1996**, *100*, 8535.
(15) Miyata, S. *Clays Clay Mater.* **1980**, *28*, 50.
(16) Sato, T.; Fujita, H.; Endo, T.; Shimada, M. *React. Solids* **1988**, *5*, 219.
(17) Velu, S.; Swamy, C. S. *Appl. Catal., A* **1994**, *119*, 241.
(18) Kruissink, E. C.; van Reijen, L. L.; Ross, J. R. H. *J. Chem. Soc., Faraday Trans. 1* **1981**, *77*, 649.
(19) Labajos, F. M.; Rives, V.; Ulibarri, M. A. *Spectrosc. Lett.* **1991**, *24*, 499.
(20) Clause, O.; Gazzano, M.; Trifiro, F.; Vaccari, A.; Zatorski, L. *Appl. Catal.* **1991**, *73*, 217.
(21) Tsuji, M.; Mao, G.; Yoshida, T.; Tamaura, Y. *J. Mater. Res.* **1993**, *8*, 1137.
(22) Thevenot, F.; Szymanski, R.; Chaumette, P. *Clays Clay Mater.* **1989**, *37*, 396.
(23) Crespo, I.; Barriga, C.; Rives, V.; Ulibarri, M. A. *Solid State Ionics* **1997**, *101−103*, 729.
(24) Ulibarri, M. A.; Fernandez, J. M.; Labajos, F. M.; Rives, V. *Chem. Mater.* **1991**, *3*, 626.
(25) Kannan, S.; Swamy, C. S. *J. Mater. Sci.* **1997**, *32*, 1623.
(26) Fetter, G.; Olgufn, M. T.; Bosch, P.; Lara, V. H.; Bulbulian, S. *J. Radioanal. Nucl. Chem.* **1999**, *241*, 595.
(27) Kamath, P. V.; Therese, H. A.; Gopalakrishnan, J. *J. Solid State Chem.* **1997**, *128*, 38.
(28) Meyn, M.; Beneke, K.; Lagaly, G. *Inorg. Chem.* **1990**, *29*, 5201.
(29) (a) Miyata, S. *Clays Clay Miner.* **1983**, *31*, 305. (b) Kooli, F.; Chisem, I. C.; Vucelic, M.; Jones, W. *Chem. Mater.* **1996**, *8*, 1969. (c) Carrado, K. A.; Forman, J. E.; Botto, R. E.; Winans, R. E. *Chem. Mater.* **1993**, *5*, 472. (d) del Arco, M.; Gutierrez, S.; Martin, C.; Rives, V.; Rocha, J. *J. Solid State Chem.* **2000**, *151*, 272. (e) Hou, X.; Kirkpatrick, R. J.; Ping Y.; Moore, D.; Kim, Y. *Am. Mineral.* **2000**, *85*, 173.
(30) Kuma, K.; Paplawsky, W.; Gedulin, B.; Arrhenius, G. *Origins Life Evol. Biosphere* **1989**, *19*, 573.
(31) Powder Diffraction File Card No. 12-0460; Joint Committee on Powder Diffraction Standards, Swarthmore, PA, 1995.
(32) Moeller, T.; Bailar, J. C., Jr.; Kleinberg, J.; Guss, C. O.; Castellion, M. E.; Metz, C. *Chemistry with Inorganic Qualitative Analysis*; Academic Press: New York, 1990; p A23.
(33) Newman, S. P.; Jones, W. *J. Solid State Chem.* **1999**, *148*, 26.
(34) (a) Delahaye-Vidal, A.; Ehlsissen, K. T.; Genin, P.; Figlarz, M. *Eur. J. Solid State Inorg. Chem.* **1994**, *31*, 823. (b) Ehlsissen, K. T.; Delahaye-Vidal, A.; Genin, P.; Figlarz, M.; Willmann, P. *J. Mater. Chem.* **1993**, *3*, 883.
(35) Rajamathi, M.; Kamath, P. V.; Seshadri, R. *Mater. Res. Bull.* **2000**, *35*, 271.
(36) Faure, C.; Delmas, C.; Willmann, P. *J. Power Sources* **1991**, *36*, 497.
(37) Pesic, L.; Salipurovic, S.; Markovic, V.; Vucelic, D.; Kagunya, W.; Jones, W. *J. Mater. Chem.* **1992**, *2*, 1069.
(38) (a) Gadsden, J. A. *Infrared Spectra of Minerals and Related Inorganic Compounds*; Butterworth: London, 1975; pp 21−24. (b) Nakamoto, K. *Infrared and Raman Spectra of Inorganic and Coordination Compounds, Part A*, 5th ed.; John Wiley and Sons: New York, 1997.
(39) (a) Labajos, F. M.; Rives, V. *Inorg. Chem.* **1996**, *35*, 5313. (b) Rey, F.; Fornes, V.; Rojo, J. M. *J. Chem. Soc., Faraday Trans.* **1992**, *88*, 2233.
(40) (a) Bensi, H. A. *J. Chem. Phys.* **1959**, *30*, 852. (b) Xu, Z. P.; Zeng, H. C. *Chem. Mater.* **2000**, in press.
(41) Hernandez-Moreno, M. J.; Ulibarri, M. A.; Rendon, J. L.; Serna, C. J. *Phys. Chem. Miner.* **1985**, *12*, 34.
(42) Labajos, F. M.; Rives, V.; Ulibarri, M. A. *J. Mater. Sci.* **1992**, *27*, 1546.
(43) Kannan, S.; Velu, S.; Ramkumar, V.; Swamy, C. S. *J. Mater. Sci.* **1995**, *30*, 1462.
(44) Pausch, I.; Lohse, H. H.; Schurmann K.; Allmann, R. *Clays Clay Miner.* **1986**, *34*, 507.
(45) Kannan, S.; Swamy, C. S. *J. Mater. Sci. Lett.* **1992**, *11*, 1585.
(46) *Handbook of Chemistry and Physics*, 80th ed.; Lide, D. R., Ed.; CRC: Boca Raton, FL, 1999; pp 9−11.
(47) Kleinberg, J. B.; Argersinger, W. J., Jr.; Griswold, E. *Inorganic Chemistry*; D. C. Heath and Co.: Boston, MA, 1960; p 356.
(48) van der Pol, A.; Mojet, B. L.; van der Ven, E.; de Boer, E. *J. Phys. Chem.* **1994**, *98*, 4050.
(49) Kirkpatrick, R. J.; Ping, Y.; Hou, X.; Kim, Y. *Am. Mineral.* **1999**, *84*, 1186.